Atomic-Scale Influence of Grain Boundaries on Li-Ion Conduction in Solid Electrolytes for All-Solid-State Batteries

James A. Dawson,*,[†] Pieremanuele Canepa,[†] Theodosios Famprikis,[†,‡] Christian Masquelier,[‡] and M. Saiful Islam*,[†]

[†]Department of Chemistry, University of Bath, Bath BA2 7AY, U.K.

[‡]Laboratoire de Réactivité et de Chimie des Solides (UMR CNRS 7314), Université de Picardie Jules Verne, 33 rue Saint Leu, 80039 Amiens Cedex, France

S *Supporting Information*

ABSTRACT: Solid electrolytes are generating considerable interest for all-solid-state Li-ion batteries to address safety and performance issues. Grain boundaries have a significant influence on solid electrolytes and are key hurdles that must be overcome for their successful application. However, grain boundary effects on ionic transport are not fully understood, especially at the atomic scale. The Li-rich anti-perovskite Li_3OCl is a promising solid electrolyte, although there is debate concerning the precise Li-ion migration barriers and conductivity. Using Li_3OCl as a model polycrystalline electrolyte, we apply large-scale molecular dynamics simulations to analyze the ionic transport at stable grain boundaries. Our results predict high concentrations of grain boundaries and clearly show that Li-ion conductivity is severely hindered through the grain boundaries. The activation energies for Li-ion conduction traversing the grain boundaries are consistently higher than that of the bulk crystal, confirming the high grain boundary resistance in this material. Using our results, we propose a polycrystalline model to quantify the impact of grain boundaries on conductivity as a function of grain size. Such insights provide valuable fundamental understanding of the role of grain boundaries and how tailoring the microstructure can lead to the optimization of new high-performance solid electrolytes.
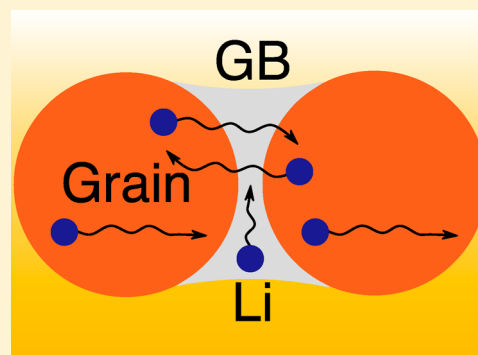
1. INTRODUCTION

Li-ion batteries have revolutionized the portable electronics industry. However, safety and cycling life issues remain a challenge for current commercial batteries based on liquid electrolytes. Significant efforts have been recently focused on the development of all-solid-state batteries,[1−9] which have the potential to eliminate the use of flammable liquid electrolytes. Nevertheless, there are challenges to overcome, such as insufficient ionic conductivity, narrow electrochemical stability windows, and interfacial issues.

Many families of materials based on NASICON, LISICON, thio-LISICON, and garnet structures have been investigated as potential solid electrolytes, each with their own particular strengths and weaknesses.[10−14] More recently, a new family of materials based on Li-rich anti-perovskites, Li_3OX (X = Cl or Br), have been receiving increasing attention.[15−21] The first study of these materials[15] as solid electrolytes showed that they possess high ionic conductivity ($>10^{-3}$ S cm^{-1} at room temperature) and low migration barriers (0.2−0.3 eV) for Li-ion transport.

Subsequently, there have been several reports of higher activation energies (~0.6 eV) and lower conductivities (10^{-6} S cm^{-1} at room temperature) for bulk Li_3OCl and Li_3OBr,[16,22−24] with some studies proposing grain boundary (GB) resistance as the reason for the differences.[16,22,24] A

remarkable amount of interest has recently been generated with reports on the creation of "glass" batteries based on Li_3OCl solid electrolytes by Braga et al.[25,26] In parallel, a number of computational studies on Li_3OCl[19,20,27−31] predict Li-ion activation energies (~0.3−0.4 eV) that are consistently lower than the experimentally determined values (~0.6 eV). The reason for this significant discrepancy is still unclear.

GB resistance in Li-ion solid electrolytes is a significant challenge that must be overcome to reach the ionic conductivities required for practical applications. However, while many reports mention the influence of GBs on the Li-ion conductivity, it is rarely quantified or characterized in detail, especially on the atomic scale. It is crucial to bear in mind that it is not possible to determine a priori whether GBs will be detrimental or beneficial for conduction in a given material.[32]

The lack of GB characterization is also true for Li_3OCl, with only a few studies briefly discussing their influence on the electrochemical performance. Lü et al.[16,22] synthesized Li_3OCl thin films with an activation energy of 0.35 eV, considerably lower than the value of 0.59 eV for the bulk material. This difference was explained by the larger grain size of the films compared to the bulk material and, as a result, the reduced GB

resistance. In addition, impedance measurements confirmed large GB resistances and lower conductivities, compared to the bulk, for a closely related anti-perovskite, Li_3OBr.[23,24]

Despite the fundamental importance of GBs in Li-based solid electrolytes, they are not fully understood. The possible pathways for Li-ion transport pathways in the grains and at the GBs, including intragranular (within grains), intergranular (between grains), and within the GB, are illustrated in Figure 1. Using large-scale molecular dynamics (MD), we explore the
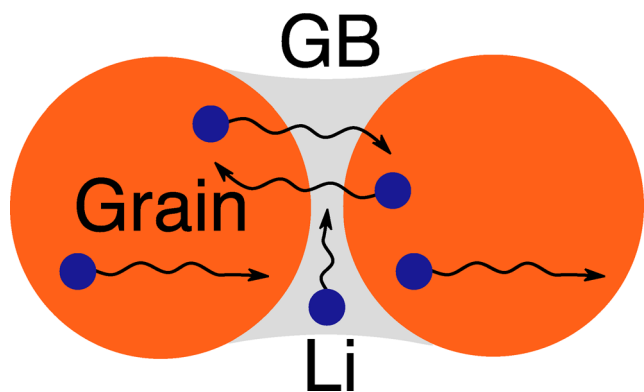

Figure 1. Schematic showing possible Li-ion (blue) transport mechanisms at the GB (gray) and grain (orange) of a solid electrolyte material.

atomistic effects of GBs on the Li-ion conductivity of a representative solid electrolyte, Li_3OCl. We show that GB formation in Li_3OCl is generally more favorable than in non-Li-based perovskites. The most stable GBs exhibit reduced Li-ion conductivities and increased activation energies compared to bulk Li_3OCl. We use our findings to reconcile the inconsistencies in activation energies between experimental and computational studies and to establish a model that can quantify the effects of GBs on the overall conductivity of polycrystalline solid electrolytes. Our results provide valuable atomic-scale insights into the role of GBs on the Li-ion transport performance of solid electrolytes.

2. METHODS

The MD simulations are based on established techniques and have been widely used to determine the ion transport properties in a wide range of ionic solids,[33−37] extending our recent work on battery materials.[38,39] The potential model of Mouta et al.[29] was used for the calculations, with a number of additions[40−42] (see Table S1) to produce the best agreement in terms of lattice parameters and bond lengths of the Li_3OCl anti-perovskite structure. Formal valence charges were used for all ions, and a cutoff of 12 Å was applied to all interatomic potentials.

The LAMMPS code[43] was used for the MD calculations, with periodic boundary conditions. Significantly long MD runs of 10 ns were completed using a time step of 2 fs with supercells of 5076 ions for both the bulk and GBs. Simulations were carried out for a temperature range of 500−1000 K at intervals of 100 K using the NVT ensemble with a Nose-Hoover thermostat,[44] with initial equilibration performed using the NPT ensemble for several nanoseconds. It is generally accepted in the literature that Li vacancies are the dominant charge carriers in Li_3OCl and are compensated for by Cl vacancies.[16,20,27,29] Disorder was introduced to the systems to aid long-range diffusion using Li and Cl vacancies that were randomly distributed throughout the supercells at representative concentrations of 3.33% and 10%, respectively. Self-diffusion data for Li were obtained from a mean squared displacement (MSD) analysis according to

$$\langle r_i^2(t) \rangle = 6D_{Li}t \qquad (1)$$

where $\langle r_i^2(t) \rangle$ is the MSD, D_{Li} is the diffusion coefficient for Li, and t is time. The diffusion data were then converted to conductivities (σ) using the Nernst−Einstein relationship:

$$\frac{\sigma}{D_{Li}} = H_R \frac{nq^2}{kT} \qquad (2)$$

where n is the number of charge carriers per unit volume, q is the electron charge, k is the Boltzmann constant, T is the temperature, and H_R is the Haven ratio, which has a value of 1 in our calculations.

The coherent, twin GBs were constructed using the coincidence site lattice theory[45] where two individual grains are tilted by a given angle until their surface planes coincide, as shown schematically in Figure 2. We consider four symmetric tilt GBs, namely, $\Sigma3(111)$,
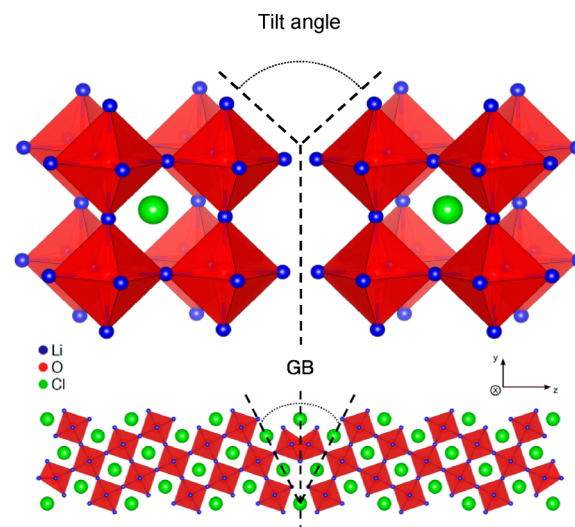

Figure 2. Schematic of the GB construction process using the cubic anti-perovskite Li_3OCl structure, in which Li, O, and Cl ions occupy the X, B, and A sites of the ABX_3 perovskite structure. GBs are constructed using the coincidence site lattice theory where two individual grains are rotated by a given tilt angle until their surface planes coincide.[45] To avoid ambiguity, we define here GBs as the surfaces between two crystallites (grains) of different orientations. Such GBs can exist within a polycrystalline particle, which make up a ceramic.

$\Sigma3(112)$, $\Sigma5(210)$, and $\Sigma5(310)$, as shown in Figure 3. In this notation, Σ is the coincidence index and is the ratio of the coincidence unit cell volume to the primitive unit cell volume.[45] These common GBs were chosen as they have been observed for a variety of perovskite samples, including $BaTiO_3$, $SrTiO_3$, and $BaZrO_3$.[46,47] Such a characterization does not exist for Li_3OCl.

We explored the potential energy surfaces of the four initial GBs to find the global minimum for each structure. For each translation, the GB energy, γ_{GB}, is derived by

$$\gamma_{GB} = \frac{E_{GB} - E_{bulk}}{2A} \qquad (3)$$

where E_{GB} and E_{bulk} are the energies of the GB and bulk supercells, respectively, and A is the area of the shared interface. The energy was calculated as a function of translation with increments of 0.1 Å. The GB energy was converged with GB separation using a variety of supercells with lengths from ~30 to 100 Å. This approach has been applied to the construction of numerous GBs in many different materials.[48−52] For the MD calculations, the GB unit cells were replicated periodically in three dimensions by 7×3×1, 6×5×1, 9×4×1, and 6×3×1 for $\Sigma3(111)$, $\Sigma3(112)$, $\Sigma5(210)$, and $\Sigma5(310)$, respectively. Each supercell was divided into GB and bulk-like (grain)
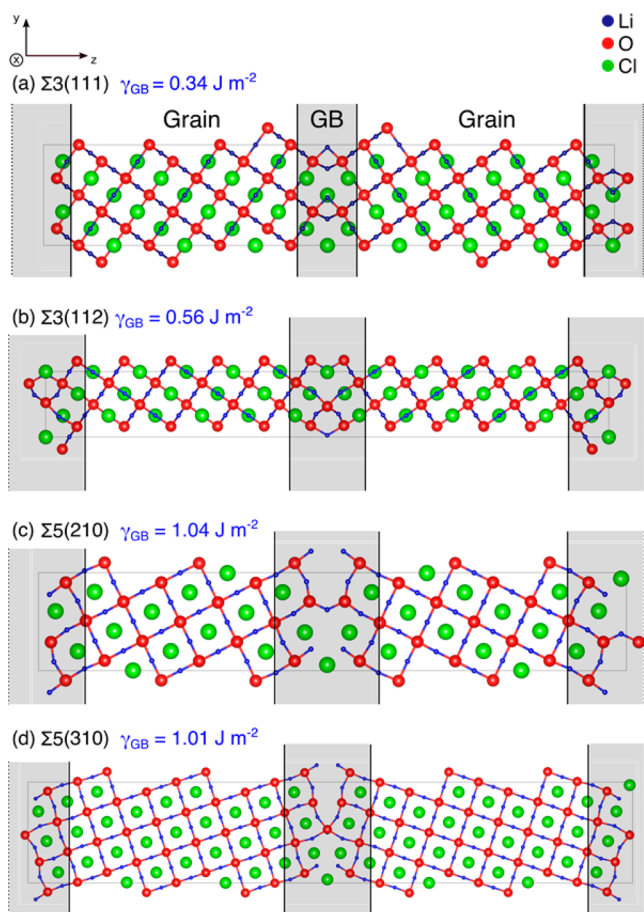
Figure 3. Structures and energies of the (a) $\Sigma 3(111)$, (b) $\Sigma 3(112)$, (c) $\Sigma 5(210)$, and (d) $\Sigma 5(310)$ GBs. Equivalent GBs are located at the center and edges of each supercell. The x and y directions represent the planes of the GBs, while the z direction is perpendicular to the GB plane.

components, as illustrated in Figure 3, in order to distinguish the contribution of the GBs to the Li-ion conductivity.

3. RESULTS AND DISCUSSION

3.1. Bulk and Grain Boundary Structures. First, the bulk anti-perovskite structure is simulated, which is comprised of oxide ions at the typical B-site of an ABX_3 perovskite coordinated to six Li^+ ions at the X sites and the large Cl ion occupying the 12-coordinate A-site, as shown in Figure 2. The calculated lattice parameter for bulk Li_3OCl is 3.919 Å, with only a 0.31% difference compared to the X-ray diffraction value of 3.907 Å,[53] as shown in Table S2.

The four optimized GB structures and their calculated energies are shown in Figure 3. The x and y directions represent the planes of the GBs, while the z direction is perpendicular to the GB plane. The cell dimensions and GB separation for each GB are given in Table S3. In general, these computed GB energies are low compared to the equivalent GBs in perovskite oxides, such as $BaTiO_3$,[54] $SrTiO_3$,[55] and $BaZrO_3$.[56]

The notably low GB energies shown in Figure 3 indicate the presence of high concentrations of GBs in Li_3OCl, as illustrated by the probability of formation plot in Figure S1, based on a Boltzmann distribution. Such high concentrations of GBs are obviously likely to contribute to the high GB resistance in the material.

On the basis of electrostatic arguments, such low GB energies are unsurprising given that the ionic charges of Li and Cl are low, meaning there is a smaller energetic penalty for cleaving Li−O and Li−Cl bonds than, for example, cleaving Ba−O and Ti−O bonds in $BaTiO_3$. In addition, first-principles calculations have shown that Li is capable of adjusting to many coordination environments.[57] These low energies suggest that GBs will form with ease in Li_3OCl samples, which is likely to be a reason for their significant influence on its Li-ion conductivity.

The lowest GB energies are calculated for the two $\Sigma 3$ GBs. This is probably due to the reduced coordination environments at the two $\Sigma 5$ GBs with open structures and the limited disruption of the bonding at the $\Sigma 3$ GBs. The large difference of >0.45 J m^{-2} between the $\Sigma 3$ and $\Sigma 5$ GB energies strongly suggests that the $\Sigma 3$ GBs will be present in far higher concentrations (see Figure S1) and will therefore influence the ionic transport of Li to a far greater extent. This is an important consideration when comparing the conductivity and resistance of the two GB types. It is also important to bear in mind that grain orientations and other microstructural restrictions are likely to limit the concentration of any one particular GB in a polycrystalline material, regardless of its thermodynamic stability.[45,58]

3.2. Li-Ion Conductivity of Bulk and Grain Boundaries. As noted, previous computational studies have not considered the effects of GBs on this system. To probe the impact of GB resistance on Li-ion conductivity in solid electrolytes using Li_3OCl as a model system, we have carried out large-scale MD simulations.

Figure 4 shows the Arrhenius plots for the calculated total Li^+ temperature-dependent ionic conductivity of each GB and
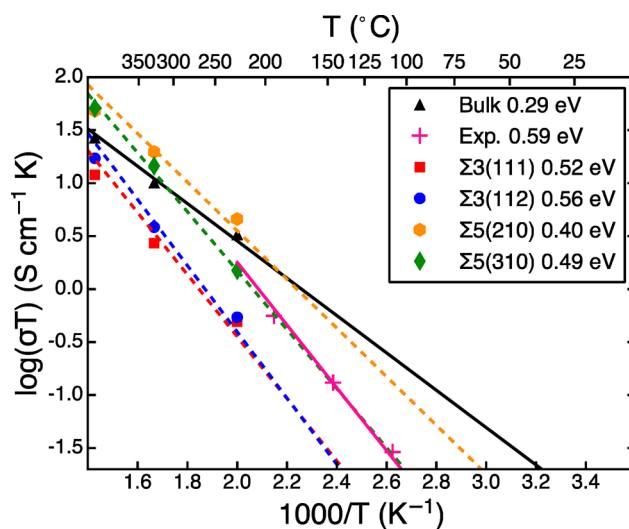

Figure 4. Li^+ temperature-dependent conductivities (σT) and activation energies (E_a) for bulk Li_3OCl and the four GBs. Electrochemical impedance spectroscopy results are included for comparison.[22] The complete set of simulated Li-ion conductivities is presented in Figure S3.

bulk Li_3OCl. Electrochemical impedance spectroscopy measurements are also included for comparison.[22] MSD plots for Li-ion diffusion in bulk Li_3OCl and for the four GBs at a representative temperature of 700 K are given in Figure S2. The Li-ion conductivity of the four GBs and the experimentally measured values are lower than the bulk values at normal

battery operating temperatures (~0 to 150 °C). This confirms the high GB resistance in Li$_3$OCl. However, it is interesting to note that at higher temperatures (>500 K), the conductivities of the Σ5 grain boundaries exceed those of the bulk material.

The calculated bulk Li$_3$OCl conductivity is 6.55×10^{-3} S cm^{-1} at 500 K, in good agreement with experimental studies.[15,22] It should be noted that as a result of different synthesis and sample preparation techniques, a wide range of electrochemical impedance spectroscopy measurements have been reported in the literature.[24] From our calculations, there is significant variation in conductivity for the GBs, with about a 1 order of magnitude difference between the lowest value of 9.85×10^{-4} S cm^{-1} obtained for Σ3(111) and the highest value of 9.17×10^{-3} S cm^{-1} found for Σ5(210) at 500 K. The only quantitative measurement of the GB conduction in these materials was completed for Li$_3$OBr,[24] with bulk and GB conductivities of 1.02×10^{-5} and 1.09×10^{-6} S cm^{-1}, respectively, at 298 K. Furthermore, Zhu et al.[23] reported that GB resistance dominates the total impedance of Li$_3$OBr, as illustrated by bulk and GB resistances of 8.8 and 83.0 kΩ, respectively, measured using electrochemical impedance spectroscopy.

The calculated activation energy of 0.29 eV for bulk Li$_3$OCl is in good agreement with previous calculations.[20,27] However, this value and those calculated previously all significantly underestimate the electrochemical impedance spectroscopy measured values of ~0.6 eV.[16,22−24] Until now, this discrepancy between experiment and calculations has been unexplained. Our results highlight the importance in directly considering GB contributions to conductivity in anti-perovskite solid electrolytes, and this is indeed the case for many other solid electrolyte materials.

Chemically, GBs in oxides are known to play a key role in defining the electrochemical performance of a material, whereas reports of low GB resistance in sulfide solid electrolytes suggest that GBs have less of an impact in these materials.[59−61] Furthermore, recent reports on the formation of glassy solid electrolytes without the presence of GBs present another interesting research direction.[25,26] The importance of GBs in sintering is another important aspect that should be considered in the preparation of solid electrolyte materials, since GBs can cause defect segregation or act as diffusion pathways.[62] In addition, the difference between bulk and GB domains has been proposed as the reason for the nucleation of Li dendrites when a Li-metal anode is utilized.[63] On this basis, our future calculations will seek to address potential ion redistribution, defect segregation, and space-charge effects[64,65] at the interfaces of Li-ion solid electrolytes.

3.3. Pathways of Li-Ion Conduction. The spatial dependence of the conductivity at the lowest energy GB, Σ3(111), can be visualized by analyzing the Li-ion trajectories of the simulations to produce Li-ion density maps, as shown in Figure 5. It can be seen that the Li-ion transport is restricted primarily to the x and y directions, i.e., close to the GB. Within the GB, the Li ions are free to move as a result of the reduced atomic density and are not constrained by the need for vacant Li sites in order to diffuse through the lattice, as is the case for bulk Li$_3$OCl. Over time, some of the Li ions that were restricted to the GB propagate into the bulk region of the grain. By 10 ns, they begin to form trajectory plots similar to those observed for vacancy migration in bulk Li$_3$OCl, as seen by the cubic patterns. Such results indicate the importance of
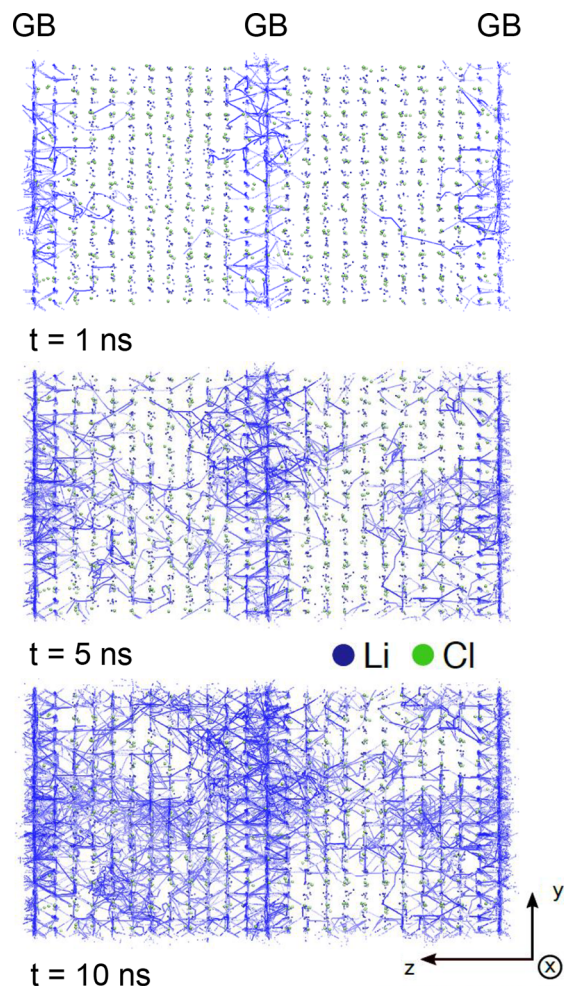

Figure 5. Trajectory plots of Li$^+$ conductivity for the Σ3(111) GB at 700 K at 1, 5, and 10 ns, where x and y are the planes of the GBs and z is perpendicular to the GB plane. Oxygen ions have been omitted for clarity.

characterizing and analyzing individual GBs, as their impact on ionic transport can vary significantly.

While the trends in conduction vary depending on the type of GB, the increase in activation energy from the bulk to the GBs occurs in all cases. Figure 6 displays the differences between the GB activation energies in the three primary directions and the bulk value, which indicates that the increase in activation energy is regardless of the GB type and conduction direction. The fact that these energy differences are all positive values clearly illustrates the significant effect of GB resistance on the ionic transport in solid electrolytes. High activation energies of 0.52 and 0.56 eV, respectively, are obtained for the dense Σ3(111) and (112) GBs. As noted previously, the Σ3(111) and (112) GBs are thermodynamically more accessible (Figures 3 and S1) and are likely to be present in higher concentrations, which means that the ionic transport resistance from these GBs will dominate.

3.4. From Atomistic Insight to a Polycrystalline Model. Using our calculated conductivities, we built a phenomenological model to rationalize the effects of GBs on the overall ionic conductivity of a real polycrystalline sample. This general model enhances our predictive capabilities by explicitly accounting for the influence of grain size by combining the contributions from bulk and GB conductivities.
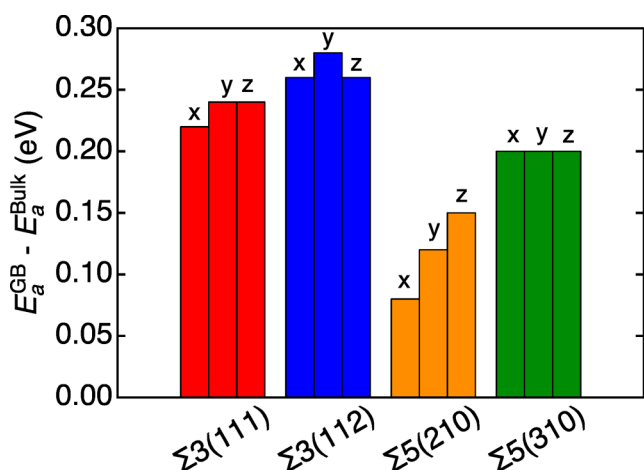
Figure 6. Differences between the GB activation energies (E_a^{GB}) in the three primary directions and the bulk value (E_a^{Bulk}, 0.29 eV), with *x* and *y* as the planes of the GBs and *z* perpendicular to the GB plane.

Our model is derived from a general equivalent circuit, routinely used in the interpretation of electrochemical impedance data,[66,67] as shown in eq 4:

$$\sigma_{total} = y_{bulk}\left(\sigma_{bulk} + \frac{d}{l_{GB}}\sigma_{GB\perp}\right) + y_{GB}\sigma_{GB\parallel} \tag{4}$$

where σ_{total} and σ_{bulk} are the total and bulk conductivities, respectively, and $\sigma_{GB\perp}$ and $\sigma_{GB\parallel}$ are the GB conductivities perpendicular and parallel to the grain, respectively, as taken from our calculations. *d* is the grain size (which can vary in our model), l_{GB} is the length of the GB, and y_{bulk} and y_{GB} control the volume fraction of the grain and GB domains, respectively. The full derivation of eq 4 is given in the SI.

Figure 7 depicts the two competing pathways of ionic conduction in a polycrystalline solid electrolyte.[32] The
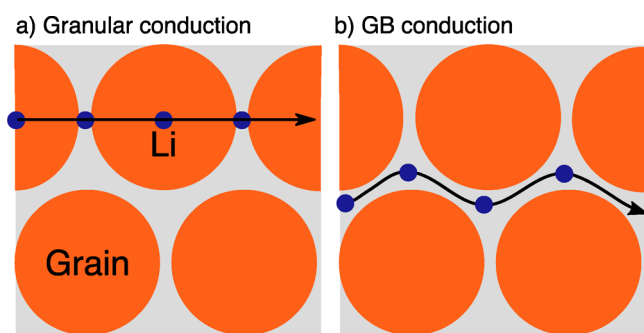

Figure 7. Schematic of the two competing mechanisms for conduction in polycrystalline materials: (a) granular and (b) GB. The orange and gray areas represent the monocrystalline grains and effective GB regions, respectively, while blue circles are mobile Li⁺ ions.

"granular" pathway (Figure 7a) represents the Li-ion conduction through the grains and GBs, and will dominate when the GBs are more resistive than the bulk crystalline structure, as is the case for Li_3OCl. The "GB" pathway (Figure 7b) will dominate when the GB conduction is comparable to that in the bulk structure, as reported for sulfides[61] and some solid oxide electrolytes, such as the garnet-structured $Li_7La_3Zr_2O_{12}$.[8,68]

The dependence of the total conductivity of a polycrystalline sample of Li_3OCl, derived using eq 4, is plotted against grain size, *d*, in Figure 8. The total conductivity originating from our
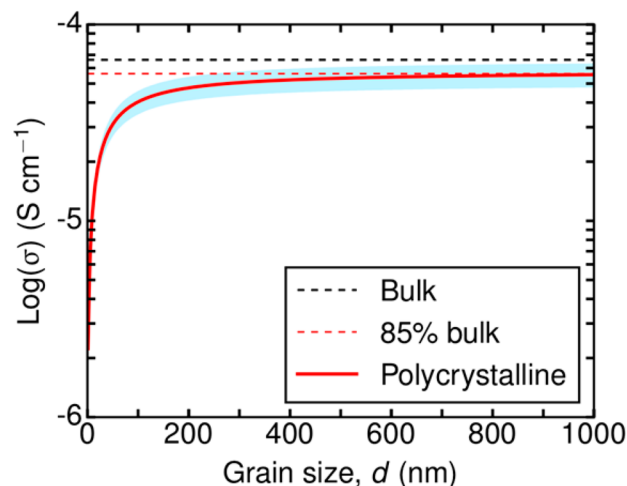

Figure 8. Evolution of the total conductivity (bulk + polycrystalline) as a function of grain size, *d* (in nm), for Li_3OCl at 300 K. The black dashed line is the calculated bulk conductivity. The red curve is the total conductivity of the polycrystalline material, with the blue band representing its upper and lower limits based on different densification behaviors (see SI for details). The red dashed line is the maximum average polycrystalline conductivity, equivalent to 85% of the bulk conductivity.

model is plotted in red, while the black dashed line identifies the bulk conductivity ($\sim6.6 \times 10^{-5}$ S cm⁻¹). From our analysis, the total conductivity above a $\sim$500 nm grain size is marked by a red dashed line and corresponds to $\sim$85% of the bulk conductivity. The blue band around the average polycrystalline conductivity represents two extreme cases calculated based on different densification behaviors (see SI for further details).

Figure 8 reveals three main features. First, the Li-ion conductivity in the polycrystalline material increases with increasing grain size, as expected given the significant resistance of the GBs shown in this work. Second, the influence of GB resistance is strongest at very small grain sizes of <100 nm, with the onset of bulk conductivity occurring within $\sim$400 nm, as identified by the upper bound of the blue band. Third, for grain sizes <100 nm, the total conductivity is dominated by the GBs, as illustrated in Figure 7b.

In this work, the conductivity computed for Li_3OCl is negatively impacted by the presence of GBs, and this is likely to be common in ceramic solid electrolytes.[8,32] Due to the low GB energies (see Figure 3) in Li_3OCl, we show that the microstructure of polycrystalline anti-perovskite samples should be sensitive to the processing conditions (synthesis and densification). It has been reported that slow crystallization from the melt and/or sintering results in sizable grains and higher conductivity in this material.[15,22]

In addition, we speculate that our model can be extended to other polycrystalline materials and to assess how the GB ionic conductivity may be beneficial for materials that show sluggish Li kinetics. In contrast, completely amorphous solid electrolytes, such as LiPON,[69] would be unaffected by such effects of blocking GBs.

5. CONCLUSIONS

The atomistic effects of grain boundaries are important to fully understand the transport properties of solid electrolytes for all-solid-state batteries. In this study, we have quantified the impact of grain boundaries in a model solid electrolyte material, Li_3OCl, using large-scale MD simulations. The results reveal the following key features:

(1) The low grain boundary energies indicate the presence of high grain boundary concentrations in polycrystalline samples of Li_3OCl. The calculated bulk ionic conductivity is 6.55×10^{-3} S cm^{-1} at 500 K, in good agreement with experimental studies. The most thermodynamically stable grain boundaries exhibit Li-ion conductivities ($\sim 10^{-4}$ S cm^{-1} at 500 K) about 1 order of magnitude lower than the bulk, indicating grain boundary resistance.

(2) There is an increase in the Li-ion migration activation energy for all grain boundaries ($0.40-0.56$ eV) compared to the bulk (0.29 eV). These results help to rationalize why previously calculated activation energies for bulk anti-perovskites have been consistently underestimated compared to experiment.

(3) From our atomistic calculations, we can develop a polycrystalline model to optimize the ionic conductivity on the basis of grain size, thereby leading to the effective sintering of Li_3OCl and other solid electrolytes.

The atomic-scale insights presented here quantify grain boundary resistance in a solid electrolyte for Li-ion battery applications and are generally applicable to a range of materials. Enhancing our fundamental understanding of these interfaces and their influence on Li-ion transport is crucial for the future optimization of new solid electrolytes for all-solid-state batteries.

■ ASSOCIATED CONTENT

Ⓢ Supporting Information

The Supporting Information is available free of charge on the ACS Publications website at DOI: 10.1021/jacs.7b10593.

Tables S1−S5 listing potential model parameters, structural parameters, supercell dimensions and parameters used in polycrystalline conductivity model; Figures S1−S4 showing Boltzmann distribution of GBs, MSDs of the bulk and GBs, Arrhenius plots, and the direct current circuit; description of the total conductivity model derivation (PDF)

■ AUTHOR INFORMATION

Corresponding Authors

*j.a.dawson@bath.ac.uk
*m.s.islam@bath.ac.uk

ORCID Ⓞ

James A. Dawson: 0000-0002-3946-5337
Pieremanuele Canepa: 0000-0002-5168-9253
Christian Masquelier: 0000-0001-7289-1015
M. Saiful Islam: 0000-0003-3882-0285

Notes

The authors declare no competing financial interest.

■ REFERENCES

(1) Manthiram, A.; Yu, X.; Wang, S. *Nat. Rev. Mater.* **2017**, *2*, 16103.
(2) Janek, J.; Zeier, W. G. *Nat. Energy* **2016**, *1*, 16141.
(3) Tikekar, M. D.; Choudhury, S.; Tu, Z.; Archer, L. A. *Nat. Energy* **2016**, *1*, 16114.
(4) Li, J.; Ma, C.; Chi, M.; Liang, C.; Dudney, N. J. *Adv. Energy Mater.* **2015**, *5*, 1401408.
(5) Bachman, J. C.; Muy, S.; Grimaud, A.; Chang, H.-H.; Pour, N.; Lux, S. F.; Paschos, O.; Maglia, F.; Lupart, S.; Lamp, P.; Giordano, L.; Shao-Horn, Y. *Chem. Rev.* **2016**, *116*, 140.
(6) Masquelier, C. *Nat. Mater.* **2011**, *10*, 649.
(7) Kamaya, N.; Homma, K.; Yamakawa, Y.; Hirayama, M.; Kanno, R.; Yonemura, M.; Kamiyama, T.; Kato, Y.; Hama, S.; Kawamoto, K.; Mitsui, A. *Nat. Mater.* **2011**, *10*, 682.
(8) Ma, C.; Chi, M. *Front. Energy Res.* **2016**, *4*, 23.
(9) Wang, Y.; Richards, W. D.; Ong, S. P.; Miara, L. J.; Kim, J. C.; Mo, Y.; Ceder, G. *Nat. Mater.* **2015**, *14*, 1026.
(10) Goodenough, J. B.; Hong, H. Y.-P.; Kafalas, J. A. *Mater. Res. Bull.* **1976**, *11*, 203.
(11) Bruce, P. G.; West, A. R. *J. Electrochem. Soc.* **1983**, *130*, 662.
(12) Kanno, R.; Hata, T.; Kawamoto, Y.; Irie, M. *Solid State Ionics* **2000**, *130*, 97.
(13) Thangadurai, V.; Kaack, H.; Weppner, W. J. F. *J. Am. Ceram. Soc.* **2003**, *86*, 437.
(14) Knauth, P. *Solid State Ionics* **2009**, *180*, 911.
(15) Zhao, Y.; Daemen, L. L. *J. Am. Chem. Soc.* **2012**, *134*, 15042.
(16) Lü, X.; Howard, J. W.; Chen, A.; Zhu, J.; Li, S.; Wu, G.; Dowden, P.; Xu, H.; Zhao, Y.; Jia, Q. *Adv. Sci.* **2016**, *3*, 1500359.
(17) Li, Y.; Zhou, W.; Xin, S.; Li, S.; Zhu, J.; Lü, X.; Cui, Z.; Jia, Q.; Zhou, J.; Zhao, Y.; Goodenough, J. B. *Angew. Chem., Int. Ed.* **2016**, *55*, 9965.
(18) Hood, Z. D.; Wang, H.; Samuthira Pandian, A.; Keum, J. K.; Liang, C. *J. Am. Chem. Soc.* **2016**, *138*, 1768.
(19) Zhang, Y.; Zhao, Y.; Chen, C. *Phys. Rev. B: Condens. Matter Mater. Phys.* **2013**, *87*, 134303.
(20) Lu, Z.; Chen, C.; Baiyee, Z. M.; Chen, X.; Niu, C.; Ciucci, F. *Phys. Chem. Chem. Phys.* **2015**, *17*, 32547.
(21) Sagotra, A. K.; Errandonea, D.; Cazorla, C. *Nat. Commun.* **2017**, *8*, 963.
(22) Lu, X.; Wu, G.; Howard, J. W.; Chen, A.; Zhao, Y.; Daemen, L. L.; Jia, Q. *Chem. Commun.* **2014**, *50*, 11520.
(23) Zhu, J.; Li, S.; Zhang, Y.; Howard, J. W.; Lü, X.; Li, Y.; Wang, Y.; Kumar, R. S.; Wang, L.; Zhao, Y. *Appl. Phys. Lett.* **2016**, *109*, 101904.
(24) Li, S.; Zhu, J.; Wang, Y.; Howard, J. W.; Lü, X.; Li, Y.; Kumar, R. S.; Wang, L.; Daemen, L. L.; Zhao, Y. *Solid State Ionics* **2016**, *284*, 14.
(25) Braga, M. H.; Murchison, A. J.; Ferreira, J. A.; Singh, P.; Goodenough, J. B. *Energy Environ. Sci.* **2016**, *9*, 948.
(26) Braga, M. H.; Grundish, N. S.; Murchison, A. J.; Goodenough, J. B. *Energy Environ. Sci.* **2017**, *10*, 331.
(27) Deng, Z.; Radhakrishnan, B.; Ong, S. P. *Chem. Mater.* **2015**, *27*, 3749.
(28) Emly, A.; Kioupakis, E.; Van der Ven, A. *Chem. Mater.* **2013**, *25*, 4663.
(29) Mouta, R.; Melo, M. Á. B.; Diniz, E. M.; Paschoal, C. W. A. *Chem. Mater.* **2014**, *26*, 7137.
(30) Stegmaier, S.; Voss, J.; Reuter, K.; Luntz, A. C. *Chem. Mater.* **2017**.29433010.1021/acs.chemmater.7b00659

(31) Chen, M.-H.; Emly, A.; Van der Ven, A. *Phys. Rev. B: Condens. Matter Mater. Phys.* **2015**, *91*, 214306.

(32) Dufour, L. C.; Monty, C. *Surfaces and Interfaces of Ceramic Materials*; Kluwer Academic Publishers: Dordrecht, 1989.

(33) Islam, M. S.; Fisher, C. A. *J. Chem. Soc. Rev.* **2014**, *43*, 185.

(34) Catlow, C. R. A. *Computational Approaches to Energy Materials*; Wiley: Chichester, 2013.

(35) Deng, Y.; Eames, C.; Fleutot, B.; David, R.; Chotard, J.-N.; Suard, E.; Masquelier, C.; Islam, M. S. *ACS Appl. Mater. Interfaces* **2017**, *9*, 7050.

(36) Deng, Y.; Eames, C.; Chotard, J.-N.; Lalère, F.; Seznec, V.; Emge, S.; Pecher, O.; Grey, C. P.; Masquelier, C.; Islam, M. S. *J. Am. Chem. Soc.* **2015**, *137*, 9136.

(37) Chen, C.; Du, J. *J. Am. Ceram. Soc.* **2015**, *98*, 534.

(38) Armstrong, A. R.; Lyness, C.; Panchmatia, P. M.; Islam, M. S.; Bruce, P. G. *Nat. Mater.* **2011**, *10*, 223.

(39) Tompsett, D. A.; Parker, S. C.; Islam, M. S. *J. Am. Chem. Soc.* **2014**, *136*, 1418.

(40) Islam, M.; Read, M. S. D.; D'Arco, S. *Faraday Discuss.* **1997**, *106*, 367.

(41) Catlow, C. R. A.; Diller, K. M.; Norgett, M. J. *J. Phys. C: Solid State Phys.* **1977**, *10*, 1395.

(42) Binks, D. J. Ph.D. Thesis, University of Surrey, Guildford, UK, 1994.

(43) Plimpton, S. *J. Comput. Phys.* **1995**, *117*, 1.

(44) Evans, D. J.; Holian, B. L. *J. Chem. Phys.* **1985**, *83*, 4069.

(45) Priester, L. *Grain Boundaries: From Theory to Engineering*; Springer: New York, 2013.

(46) Ernst, F.; Mulvihill, M. L.; Kienzle, O.; Rühle, M. *J. Am. Ceram. Soc.* **2001**, *84*, 1885.

(47) Iguchi, F.; Yamada, T.; Sata, N.; Tsurui, T.; Yugami, H. *Solid State Ionics* **2006**, *177*, 2381.

(48) Benedek, N. A.; Chua, A. L.-S.; Elsässer, C.; Sutton, A. P.; Finnis, M. W. *Phys. Rev. B: Condens. Matter Mater. Phys.* **2008**, *78*, 64110.

(49) Dawson, J. A.; Tanaka, I. *J. Mater. Chem. A* **2014**, *2*, 1400.

(50) Dawson, J. A.; Tanaka, I. *ACS Appl. Mater. Interfaces* **2015**, *7*, 8125.

(51) Dawson, J. A.; Tanaka, I. *ACS Appl. Mater. Interfaces* **2014**, *6*, 17776.

(52) Moriwake, H.; Kuwabara, A.; Fisher, C. A. J.; Huang, R.; Hitosugi, T.; Ikuhara, Y. H.; Oki, H.; Ikuhara, Y. *Adv. Mater.* **2013**, *25*, 618.

(53) Reckeweg, O.; Blaschkowski, B.; Schleid, T. *Z. Anorg. Allg. Chem.* **2012**, *638*, 2081.

(54) Oyama, T.; Wada, N.; Takagi, H.; Yoshiya, M. *Phys. Rev. B: Condens. Matter Mater. Phys.* **2010**, *82*, 134107.

(55) Dawson, J. A.; Tanaka, I. *J. Phys. Chem. C* **2014**, *118*, 25765.

(56) Nyman, B. J.; Helgee, E. E.; Wahnström, G. *Appl. Phys. Lett.* **2012**, *100*, 061903.

(57) Rong, Z.; Malik, R.; Canepa, P.; Sai Gautam, G.; Liu, M.; Jain, A.; Persson, K.; Ceder, G. *Chem. Mater.* **2015**, *27*, 6016.

(58) Yang, W.; Lee, W. B. *Mesoplasticity and its Applications*; Springer: New York, 1993.

(59) Yu, C.; Ganapathy, S.; de Klerk, N. J. J.; Roslon, I.; van Eck, E. R. H.; Kentgens, A. P. M.; Wagemaker, M. *J. Am. Chem. Soc.* **2016**, *138*, 11192.

(60) Takada, K. *Acta Mater.* **2013**, *61*, 759.

(61) Seino, Y.; Ota, T.; Takada, K.; Hayashi, A.; Tatsumisago, M. *Energy Environ. Sci.* **2014**, *7*, 627.

(62) Burke, J. E. *J. Am. Ceram. Soc.* **1957**, *40*, 80.

(63) Raj, R.; Wolfenstine, J. *J. Power Sources* **2017**, *343*, 119.

(64) Maier, J. *Prog. Solid State Chem.* **1995**, *23*, 171.

(65) Zhang, Q.; Pan, J.; Lu, P.; Liu, Z.; Verbrugge, M. W.; Sheldon, B. W.; Cheng, Y.-T.; Qi, Y.; Xiao, X. *Nano Lett.* **2016**, *16*, 2011.

(66) Jamnik, J.; Maier, J. *Phys. Chem. Chem. Phys.* **2001**, *3*, 1668.

(67) Jamnik, J. *J. Electrochem. Soc.* **1999**, *146*, 4183.

(68) Murugan, R.; Thangadurai, V.; Weppner, W. *Angew. Chem., Int. Ed.* **2007**, *46*, 7778.

(69) Bates, J. B.; Dudney, N. J.; Gruzalski, G. R.; Zuhr, R. A.; Choudhury, A.; Luck, C. F.; Robertson, J. D. *Solid State Ionics* **1992**, *53*, 647.